CrystEngComm

Accepted Manuscript

CrystEngComm

PAPER

Layer-structured coordination polymers based on 5-(1H-tetrazol-5-yl)isophthalic acid: structure, sensitization of lanthanide(III) cations and small-molecule sensing

Received 00th January 20xx,
Accepted 00th January 20xx

DOI: 10.1039/x0xx00000x

www.rsc.org/

Jia Jia[a,b], Jianing Xu[a], Shengyan Wang[a], Pengcheng Wang[a], Lijuan Gao[a], Juan Chai[a], Lanlan Shen[a], Xiaobo Chen[c], Yong Fan*[a] and Li Wang*[a]

Three layer-structured coordination polymers (CPs), namely, $[Pb_2(TZI)(\mu_3\text{-}OH)(H_2O)\cdot(H_2O)]_n$ **(1)**, $[Pb(HTZI)(phen)\cdot(H_2O)]_n$ **(2)** and $[Zn_2(TZI)(\mu_3\text{-}OH)(H_2O)_2\cdot(1/2H_2O)]_n$ **(3)** have been constructed by 5-(1H-tetrazol-5-yl)isophthalic acid (H_3TZI) ligand. Notably, **1** can function as a host for encapsulation of lanthanide (III) ions and by encapsulating different Ln^{3+} ions, as-prepared Ln^{3+}@**1** materials show tunable luminescent emission including white-light emitting. Moreover, **1** exhibits highly luminescent sensing properties for organic small molecules.

Introduction

Rational design and construction of coordination polymers (CPs) have been a hot topic, given their characteristic structure, topology and specific or multifunctional properties, for instance, luminescence, gas storage and separation, catalysis, and drug delivery.[1–3] In particular, luminescent CPs are of great interest, which could be employed in diverse applications, including chemical sensors, light-emitting devices, and biomedicine.[4–6] Recently, extensive efforts have been dedicated to the design and preparation of multifunctional luminescent CP materials, in which the use of CPs as a host to encapsulate guest chromophores for fabricating luminescent host–guest materials has been advanced to a great magnitude. Especially, the encapsulation of Ln^{3+} ions with CPs not only offers a new strategy to yield tunable and white-light-emitting fluorescence materials but also for detection of small molecules.[7–19] For instance, Jiang et al. prepared a crown-ether-like, hollow Pb^{2+}-framework with subsequently intercalated Ln^{3+} ions in the cavity, which led to dual and bimodal emissions.[20] Lan et al. constructed a stable CP, $[Zn_4O(L)_3(H_2O)_2]_3\text{-}[Zn_4O(L)_3]\cdot xDMF$, namely NENU-522, ($H_2L$ = 9H-Carbazole-3,6-dicarboxylic acid, DMF = N,N-dimethylformamide, NENU = Northeast Normal University) which can emit white light by encapsulating varying molar ratios of Eu^{3+} and Tb^{3+} ions. Moreover, Tb^{3+}@NENU-522 displays a high selectivity and recyclability in the detection of nitroaromatic explosives.[10] Su and co-workers prepared a microporous anionic framework for sensing luminescence of lanthanide (III) ions and selective absorption of dyes.[21] Though such scientific advances exist, the preparation of luminescent host–guest materials remains a challenge, which can be ascribed to several limitations, such as the judicious selection of CPs and the encapsulated Ln^{3+} ions in different quantities, suitable permanent channels for encapsulation and stability of the framework in solvents.

Motivated by our interest in tunable luminescent host–guest materials, we have initiated a synthetic strategy to address the above mentioned issues. In general, the construction of CPs is determined by a number of key factors, such as nature of the central metal ions, organic carboxlate ligands, reaction temperature, and so on.[22] Of these, organic carboxylate ligands play a crucial role in establishing the construction of CPs.[23] In this regard, we chose 5-(1H-tetrazol-5-yl)isophthalic acid (H_3TZI) as a bifunctional ligand to construct functional CPs. It has been validated to be a proper polydentate bridging ligand for the formation of multidimensional coordination polymers with structural diversity.[24] In comparison to regular organic ligands, this multidentate ligand could connect multiple metallic species to increase the nuclear density of the compounds and expand spatial dimension of the CPs.[25] A good example can be seen in the use of H_3TZI ligand to generate in situ metal-organic truncated cuboctahedral supermolecular building blocks (SBBs), yielding a (24-connected)-based MOF[25a]. Moreover, four nitrogen electron-donating atoms of tetrazole group allows to serve as either a multidentate ligand or a bridging building block in assembling supramolecule,[26] and in particular, is a good candidate for enhanced emissive properties.[24] As a result, three new layer structured CPs, namely $[Pb_2(TZI)(\mu_3\text{-}OH)(H_2O)\cdot(H_2O)]_n$ **(1)**, $[Pb(HTZI)(phen)\cdot(H_2O)]_n$ **(2)** and $[Zn_2(TZI)(\mu_3\text{-}$

[a] State Key Laboratory of Inorganic Synthesis & Preparative Chemistry, College of Chemistry, Jilin University, Changchun 130012, Jilin, P. R. China. Email: lhl222@jlu.edu.cn; Fax: +86-431-85168439; Tel: +86-431-85168439
[b] College of Chemistry, Baicheng Normal University, Baicheng 137000, Jilin, P. R. China. E-mail: jj_zhx@126.com
[c] Department of Materials Science and Engineering, Monash University Clayton, VIC 3800, Australia. E-mail: xiaobo.chen@monash.edu

†Electronic Supplementary Information (ESI) available: Simulated and experimental X-ray powder diffraction pattern, UV-Vis absorption, Luminescence decay profiles, TGA curve and IR spectra. CCDC 1418713 for compound **1**, 1418704 for compound **2** and 1418639 for compound **3**. For ESI and crystallographic data in CIF or other electronic format see DOI: 10.1039/x0xx00000x

OH)(H_2O)$_2$·(1/2H_2O)]$_n$ **(3)** have been synthesized under hydrothermal conditions. They all display promising photoluminescence properties in solid state at room temperature. Notably, **1** can perform as a host for encapsulation of lanthanide (III) ions and serve as an antenna to sensitize Ln^{3+} ions, especially suitable for Eu^{3+} and Tb^{3+} ions. By encapsulating different Ln^{3+} ions, Ln^{3+}@**1** shows tunable luminescent emission including white-light emitting. In addition, **1** exhibits highly luminescent sensing properties for organic small molecules.

Experimental

Materials and Methods

All chemicals used in this work were of reagent grade. They were commercially available and used as purchased without further purification. The IR spectra (KBr pellets) were recorded in the range 400−4000 cm^{-1} on a Nicolet Impact 410 spectrometer. Elemental analyses(C, H and N) were performed on an Elementar Vario EL cube CHNOS Elemental Analyzer. UV-visible absorption spectra were recorded on a Shimadzu UV3100 spectrophotometer. Elemental analyses for Eu, Tb, Dy and Sm were obtained using a PLASMA-SPEC(I) inductively coupled plasma (ICP) atomic emission spectrometer. Thermogravimetric analyses (TGA) were carried out with a PerkinElmer TGA7 instrument, with a heating rate of 10 °C·min^{-1} under air atmosphere. Powder X-ray diffraction (XRD) measurements were performed with a D/MAX2550 diffractometer with Cu-Kα radiation (λ = 1.5418 Å) in the 2θ range of 4−40°. Photoluminescence spectra were obtained by an Edinburgh Instruments FLS 920 spectrophotometer. Energy Dispersive X-Ray Spectrometer (EDX) was performed on EDX-720. The Commission Internationale de l'Eclairage (CIE) color coordinates were calculated by following the international CIE standards.[27]

Synthesis of [Pb_2(TZI)(μ_3-OH)(H_2O)·(H_2O)]$_n$ (1)

A mixture of $Pb(NO_3)_2$ (0.0331 g, 0.1 mmol), H_3TZI (0.0234 g, 0.1 mmol), distilled water (8.0 mL) and NaOH (0.1M, 2.4 mL) was sealed in a 25 mL Teflon-lined autoclave which was then heated progressively at 120 °C for 48 h. After a gradual cooling procedure to room temperature, colorless block crystals were obtained in ca. 57.0% yield based on Pb. Anal. calcd for $C_9H_8N_4O_7Pb_2$: C, 15.47; H, 1.15; N, 8.02%. Found: C, 15.75; H, 1.22; N, 8.20%. IR (KBr, cm^{-1}): 3406(s), 2925(w), 1614(w), 1598(w), 1543(s), 1494(m), 1446(w), 1377(s), 1358(s), 1308(w), 1224(w), 1186(w), 1137(w), 1106(w), 1032(w), 922(w), 784(w), 752(s), 726(s), 674(w), 545(w), 511(w), 474(w).

Synthesis of [Pb(HTZI)(phen)·(H_2O)]$_n$ (2)

A mixture of $Pb(NO_3)_2$ (0.0331 g, 0.1 mmol), H_3TZI (0.0234 g, 0.1 mmol), 1,10-Phenanthroline (0.0198 g, 0.1 mmol) distilled water(8.0 mL) and NaOH (0.1M, 2.4 mL) was sealed in a 25 mL Teflon-lined autoclave which was then heated progressively at 140 °C for 48 h. After a gradual cooling procedure to room temperature, colorless block crystals were obtained in ca. 48.0% yield based on Pb. Anal. calcd for $C_{21}H_{14}N_6O_5Pb$: C, 39.49; H, 2.21; N, 13.17%. Found: C, 39.17; H, 2.21; N, 13.18%. IR (KBr, cm^{-1}): 3406(s), 3075(w), 1621(w), 1592(w), 1546(m), 1514(w), 1496(w), 1423(w), 1375(s), 1342(w), 1223 (w), 1187 (w), 1138(w), 1099(w), 1033(w), 926(w), 849(m), 776(w), 752(w), 727(w), 632(w), 554(w), 511(w), 482(w).

Synthesis of [Zn_2(TZI)(μ_3-OH)(H_2O)$_2$·(1/2H_2O)]$_n$ (3)

A mixture of $Zn(NO_3)_2$ (0.0297 g, 0.1 mmol), H_3TZI (0.0117 g, 0.05 mmol), distilled water (8.0 mL) and NaOH (0.5M, 0.5mL) was sealed in a 25 mL Teflon-lined autoclave which was then heated progressively at 180 °C for 72 h. After a gradual cooling procedure to room temperature, colorless block crystals were obtained in ca. 37.0% yield based on Zn. Unfortunately, the crystal of **3** is commonly small and accompanied by white impurities. To obtain the pure phase, we ever tried to adjust the molar ratios of metal ions and H_3TZI ligand or alter the pH value of the reaction system, however, the trace of white powder can be found in the final products even if the crystals were washed with distilled water for several times. Then we found the final products could be treated by ultrasonic to remove most of the impurities. Therefore, the crystals for PXRD and TGA analyses need to be manually picked. Anal. calcd for $C_9H_9N_4O_{7.5}Zn_2$: C, 25.50; H, 2.14; N, 13.22%. Found: C, 25.60; H, 2.10; N, 13.27%. IR (KBr, cm^{-1}): 3434(s), 2928(w), 1624(m), 1580(w), 1450(w), 1385(m), 1245(w), 1200(w), 1166(w), 1107(w), 926(w), 784(w), 760(w), 730(w), 603(w), 481(w).

X-ray crystallography

The crystal data of compounds **1–3** were acquired on a Rigaku R-AXIS RAPID diffractometer equipped with graphite-monochromated Mo-Kα (λ = 0.71073 Å) radiation in the ω scanning mode at room temperature. All structures were solved by direct methods and refined using full-matrix least-squares techniques with the SHELXTL software package.[28] All non-hydrogen atoms were refined anisotropically and the hydrogen atoms were placed in fixed, calculated positions using a riding model. Selected crystallographic data and refinement parameters of **1–3** are listed in Table S1, and the selected bond lengths and angles data are presented in Table S2.

Activation of 1

Before performing the experiments below, compound **1** was activated by heating the sample at 120 °C for 48 h in a vacuum oven.

Tunable luminescence

The samples of **1** (50 mg) was soaked in water solutions of nitrate salts of Eu^{3+}, Tb^{3+}, Dy^{3+}, and Sm^{3+} (5 mL, 0.1 mol/L), respectively for 48 h. Then the samples were washed with water for several times to remove residual Ln^{3+} cations on the surface and dried in air.

The solvent sensing experiment

The solvent suspensions with **1** were prepared as follows: finely ground samples of activated **1** (3 mg) was immersed into 3 mL of trichloromethane ($CHCl_3$), tetrachloromethane (CCl_4), acetonitrile (CH_3CN), ethanol (EtOH), N,N-dimethylformamide (DMF), N,N-dimethylacetamide (DMA), dichloromethane (CH_2Cl_2), tribromomethane ($CHBr_3$) and dibromomethane (CH_2Br_2), respectively. Each suspension was sonicated for 30 minutes, and then aged to form stable emulsions before their fluorescence was measured.

Results and discussion

Structural description of $[Pb_2(TZI)(\mu_3\text{-}OH)(H_2O)\cdot(H_2O)]_n$ (1)

Compound **1** crystallizes in the triclinic system with space group *P*-1.The asymmetric cell unit consists of two different Pb(II) ions, one TZI^{3-} ligand, one coordination water molecule and one free water molecule. As shown in Fig.1a, the Pb1 ion is six-coordinated by one nitrogen atom and three oxygen atoms (O3B,O4B andO2) from the two different TZI^{3-} ligands, as well as two triple-bridge oxygen atoms (O6,O6A), displaying hemi-directed $[PbNO_5]$ geometry(Fig. 1b). The Pb2 ion is seven-coordinated by one nitrogen atom and four oxygen atoms (O1, O2, O4D and O1E) from the three different TZI^{3-} ligands, one oxygen atom (O6) from the μ_3-OH^- group and one oxygen atom (O7) from the coordinated water molecule to furnish a holodirected $[PbNO_6]$ geometry (Fig. 1c).The Pb–O distances range from 2.331(8) to 2.829(9) Å, whilst the Pb1–N3 and Pb2–N4 distances are 2.668(9) and 2.618(10) Å, respectively. The benzene ring and the tetrazole ring are not in the same plane, and the dihedral angle is 35.023°.

It is worth noting that each TZI^{3-} ligand is completely deprotonated and adopts the $(\kappa^2\text{-}\kappa^1\text{-}\kappa^1\text{-}\mu_3)\text{-}(\kappa^2\text{-}\kappa^1\text{-}\mu_2)\text{-}(\kappa^1\text{-}\kappa^1\text{-}\mu_2)\text{-}\mu_9$ coordination mode (Scheme 1 a) bridging four Pb(II) ions to produce a symmetric $Pb_4(\mu_3\text{-}OH)_2(COO)_4$ tetramer cluster secondary building unit (SBU) (Fig.1d), in which the carboxylate groups from the TZI^{3-} ligand exhibit a chelating/bridging conformation and the tetrazolate moiety shows a bidentate fashion (N3C, N4C). These SBUs are further linked in different oritentations through the TZI^{3-} ligands to give rise to the formation of a 2D layered network (Fig. 1e). From the viewpoint of network topology,[29] the $Pb_4(\mu_3\text{-}OH)_2(COO)_4$ cluster connects six ligands, so it can be simplified as a 6-connected node, while the TZI^{3-} ligand can be regarded as a 3-conneced node. Therefore, the whole framework of **1** can be designated as (3, 6)-connected kgd net with the $\{4^3\}\{4^6\cdot6^6\cdot8^3\}$ topological symbol. (Fig. 1f).

Interestingly, the adjacent layers are packed through van der Waals interactions (Fig. 1g), which is different from the common molecular interactions such as hydrogen bond and π–π interaction. Such phenomenon was also reported in the references.[30-31] The distance of inter-layers is 8.115 Å and the nearest inter-layered Pb…Pb and N…N distances are approximately 4.532 Å and 6.482 Å, respectively.

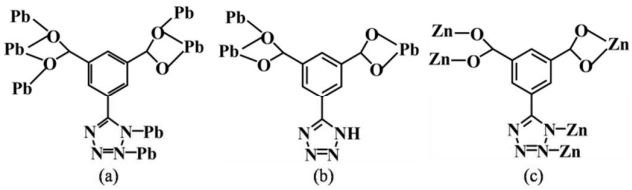

Scheme 1 Coordination modes of the TZI^{3-} ligand. Compounds **1–3** exhibit the a–c modes, respectively.

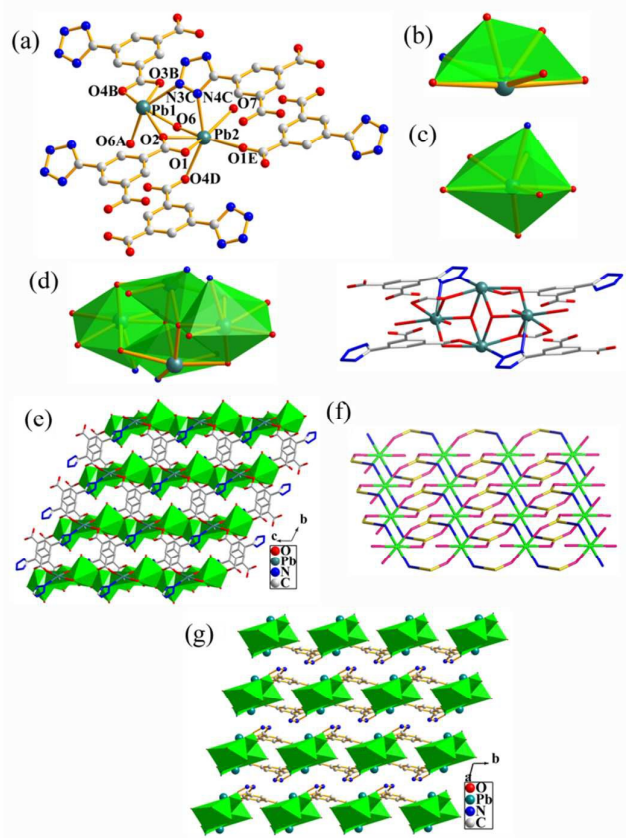

Fig.1(a) Coordination environment of Pb(II) ions in **1**. All H atoms are omitted for clarity; (b) Hemi-directed $[PbNO_5]$ geometry of Pb1 ion; (c) Holodirected $[PbNO_6]$ geometry of Pb2 ion; (d) $Pb_4(\mu_3\text{-}OH)_2(COO)_4$ tetramer cluster SBU in **1**; (e) View of 2D layer in **1** in the bc plane (hydrogen atoms and lattice water molecules are omitted for clarity); (f) Topological view showing the (3, 6)-connected kgd net for **1**; (g) The packing pattern of the adjacent layers viewed along c-axis through van der Waals interactions.

Structural description of $[Pb(HTZI)(phen)\cdot(H_2O)]_n$ (2)

Compound **2** crystallizes in the monoclinic space group $P2_1/c$. The asymmetric unit consists of one Pb(II) ion, one $HTZI^{2-}$ ligand, one phen and one free water molecule. As illustrated in Fig. 2a, the Pb1 ion is seven-coordinated by two nitrogen atoms belonging to one phen molecule and five oxygen atoms from the three different $HTZI^{2-}$ ligands to form a hemi-directed $[PbN_2O_5]$ geometry (Fig. 2b).The Pb–O distances range from 2.519(2) to 2.834(2) Å. The Pb1–N1 and Pb1–N2 distances are 2.663(3) and 2.561(3) Å, respectively. The benzene ring and the tetrazole ring of $HTZI^{2-}$ ligand are almost in the same plane with the dihedral angle of 1.828°, and it exhibits a new type of coordination mode, $(\kappa^2\text{-}\kappa^1\text{-}\mu_2)\text{-}(\kappa^2)\text{-}\mu_4$, as shown in Scheme 1b, in which the carboxylate groups from the $HTZI^{2-}$ ligand are chelating/bridging and bidentate chelating coordination modes, while the tetrazole group is not deprotonated and is not coordinated to Pb ion.

As shown in Fig.2c, two hemi-directed $[PbN_2O_5]$ polyhedra connected with each other via two bridging oxygen atoms to form a $Pb_2N_4O_8$ dimer, then adjacent dimmers are connected via bridging

$HTZI^{2-}$ ligands to form a 2D layer structure containing the rhombus windows along the [001] direction. On the basis of the concept of chemical topology, the overall structure of **2** can be assigned as a typical two-dimensional 4^4 square grid (Fig. 2d).

Strikingly, the layer structure of **2** appears to contain intertwined left and right-hand helical chains as shown in Fig. 2e. The PbN_2O_5 polyhedra and $HTZI^{2-}$ ligands through bridging atoms give rise to the helical chains of opposite chirality, which follow 2_1 screw axis with a pitch of 11.197 Å along the crystallographic X axis. These two types of helical chains are alternately connected with $Pb_2N_4O_8$ dimers functioning as the hinges, resulting in novel 2D layered network built from alternately arranged left- and right- handed helical chains in the bc-plane (Fig. 2f).

To the best of our knowledge, compound **1** and **2** are lead CPs reported for the first time in TZI system. Although the same H_3TZI ligand is used, **1** and **2** exhibit the different structure, which is attributed to the introduction of phen ligand in **2** increases the insteric hindrance, resulting in only hemi-directed geometry of Pb(II).

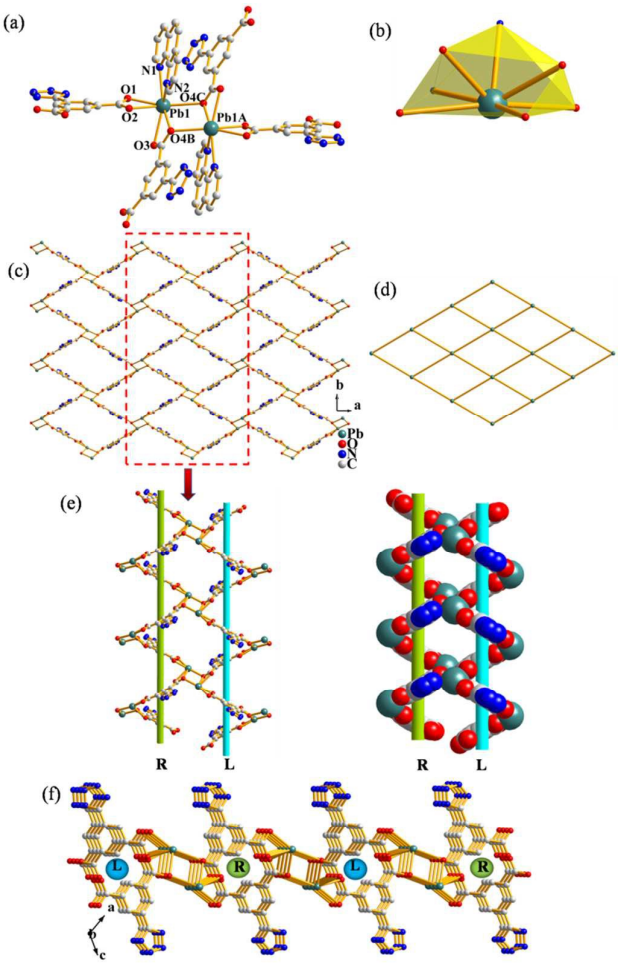

Fig.2(a) Coordination environment of Pb(II) ions in **2**. All H atoms are omitted for clarity; (b) Hemi-directed $[PbN_2O_5]$ geometry of Pb(II) ions; (c) 2D layer structure of **2** containing the rhombus windows along the [001] direction (hydrogen atoms, lattice water molecules and phen ligands are omitted for clarity); (d) Topological view showing the equivalent 2D framework of **2**; (e) View of the left and right- handed helix in **2**; (f) View of the left and right-handed helical chains formed by $HTZI^{2-}$ ligands bridging $Pb_2N_4O_8$ dimers (phen ligands are omitted for clarity).

Structural description of $[Zn_2(TZI)(\mu_3\text{-}OH)(H_2O)_2\cdot(1/2H_2O)]_n$ (3)

The asymmetric unit of **3** is shown in Fig. 3a. Different from **1,** each completely deprotonated TZI^{3-} ligand adopts the $(\kappa^1\text{-}\kappa^1\text{-}\mu_2)\text{-}(\kappa^2)\text{-}(\kappa^1\text{-}\kappa^1\text{-}\mu_2)\text{-}\mu_5$ coordination mode (Scheme 1 c) bridging four Zn(II) ions to produce a symmetric $Zn_4(\mu_3\text{-}OH)_2(COO)_4$ tetramer cluster SBU (Fig.3b), in which the carboxylate groups from the TZI^{3-} ligand exhibit a bridging and bidentate chelating coordination modes. These SBUs are further linked to form a 2D layered network (Fig. 1c). Its topological category is the same as **1** (Fig. 3d).

In compounds **1**-**3**, H_3TZI ligand exhibits three novel coordination modes (Scheme 1, a, b and c), which are never reported in the literature. So it is a good linker to construct functional CPs.[24,25a] In addition, we have prepared white light emitting and color-tunable luminescent CPs by using H_3TZI ligand and lanthanide ions in our previous work. [32]

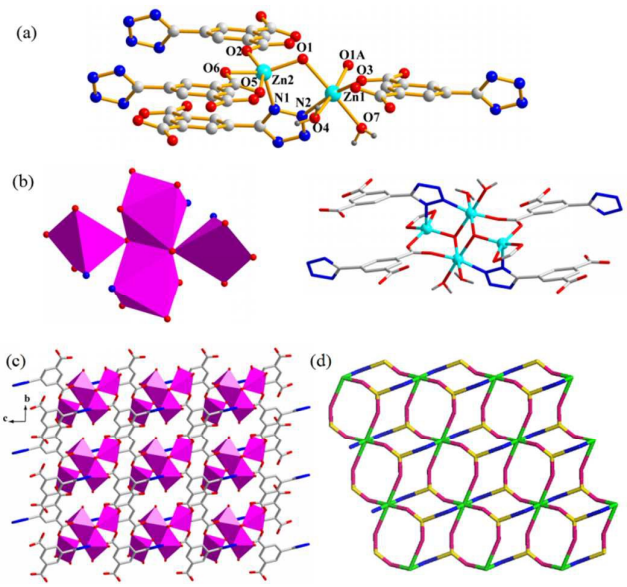

Fig.3(a) Coordination environment of Zn(II) ions in **3**; (b) $Zn_4(\mu_3\text{-}OH)_2(COO)_4$ tetramer cluster SBU in **3**; (c) View of 2D layer structure of **3** in the bc plane (hydrogen atoms and lattice water molecules are omitted for clarity); (d) Schematic representation of the (3, 6)-connected $\{4^3\}\{4^6\cdot6^6\cdot8^3\}$ topology.

Characterization

The PXRD patterns of the activated **1** and the as-synthesized sample **1** are shown in Fig. S1. It shows the activated framework almost retains its structure after the loss of water molecules. Moreover, no obvious weight loss can be found before 300 °C in the TGA curve of

the activated **1**, further confirming the water molecules have been completely removed after the activation (Fig. S2). The results of ICP and EDX analyses indicate that a similar amount of Ln^{3+} (Eu^{3+}, Tb^{3+}, Dy^{3+} or Sm^{3+}) and the different molar ratios of Eu^{3+}/Tb^{3+} have been adsorbed in the activated **1**, respectively, as summarized in Table S3-S5. Additionally, the PXRD profiles of various Ln^{3+}@**1** demonstrate their crystalline integrity can be retained after the encapsulation of Ln^{3+} ions (Fig. S3).

Photoluminescence properties of 1–3

Fig. 4 provides the luminescence spectra of compounds **1–3** in the solid state at room temperature and the excitation spectra are shown in Fig. S4. It can be observed that **1** exhibits a broad intense emission centered at 520 nm and **2** displays the emission maximum at 508 nm upon excitation at 370 nm and 320 nm, respectively. The luminescence property of the free H_3TZI ligand under the same experimental conditions was recorded for comparison. An intense emission of the free H_3TZI ligand is observed at 430 and 480 nm upon excitation at 350 nm which may be ascribed to π→π* transitions. In contrast with the luminescent properties of the free ligand, **1** and **2** show red-shift emission and are different from those of metal-centered transitions involving s and p orbitals of s^2-metal cluster compounds.[33] Therefore, the emission bands of **1** and **2** should be attributed to ligand-to-metal charge transfer (LMCT). Compound **1** and H_3TZI ligand were monitored by UV-vis absorption spectroscopy as shown in Fig. S5. In contrast to the absorbance of H_3TZI ligand, **1** showed red-shift emission and no peaks were found in visible light area. Therefore, electrons transfer to the p orbital of Pb(II) center. Since the profile of the emission band is quite similar to that of the free H_3TZI ligand, the emission of **3** could be attributed to intraligand (π–π*) emission. In addition, compared with the free ligand, the luminescent intensity of **3** is dramatically improved.

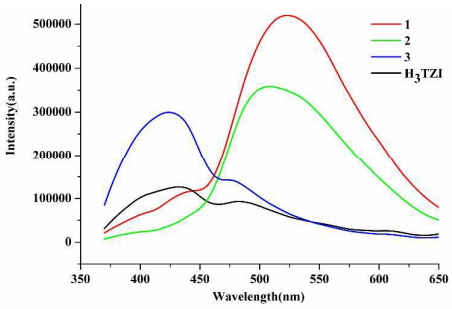

Fig. 4 Luminescence spectra of **1–3** and the H_3TZI ligand in the solid state at room temperature.

The luminescence decay curves of **1–3** were recorded at room temperature. The decay curve is well fitted into a double exponential function: $I = I_0 + A_1 \exp(-t/\tau_1) + A_2 \exp(-t/\tau_2)$, where I and I_0 are the luminescent intensities at time t = t and t = 0, respectively, whereas τ_1 and τ_2 are defined as the luminescent lifetimes (Fig. S6). The best fit of the experimental luminescence intensities to the above equation led to the following luminescence lifetimes: τ_1 = 0.73 ms and τ_2 = 4.38 ms for **1**, τ_1 = 0.35 ms and τ_2 = 2.20 ms for **2**, τ_1 = 1.58 ns and τ_2 = 4.79 ns for **3**. The obtained effective lifetime of **1** and **2** are increased compared with the lifetime of the free ligand (τ_1 = 1.37 ns and τ_2 = 5.24 ns), suggesting that they may be excellent candidates for potential photoactive materials. The fluorescence properties such as maximum emission wavelength and lifetime of organic linkers in solid MOFs are often different from those of the free molecules. This is because the organic linkers are stabilized within MOFs, which reduces the nonradiative decay rate and leads to increased fluorescence intensity and lifetimes.[34]

Tunable luminescence including white-light emission

It is well-known that the luminescence of lanthanide cations has a low molar absorptivity and that the f–f transitions are spin and parity-forbidden. Moreover, it has been shown that the lanthanide-centered emission can be sensitized by electron-conjugated systems with efficient energy-transfer, which is known as the ''antenna effect''.[35] As depicted in Fig. 5b, when excited at 350nm, Tb^{3+}@1 emitted the characteristic green luminescence of Tb^{3+}, with four characteristic bands at 488 ($^5D_4 \rightarrow {}^7F_6$), 544 ($^5D_4 \rightarrow {}^7F_5$), 583 ($^5D_4 \rightarrow {}^7F_4$), and 620 ($^5D_4 \rightarrow {}^7F_3$) nm. The most intense emission at 544 nm is attributed to the $^5D_4 \rightarrow {}^7F_5$ transition of the Tb^{3+} ion. As for Eu^{3+}@1, emissions at 579, 590, 616, 652 and 698nm were observed, which can be assigned to the characteristic $^5D_0 \rightarrow {}^7F_0$, $^5D_0 \rightarrow {}^7F_1$, $^5D_0 \rightarrow {}^7F_2$, $^5D_0 \rightarrow {}^7F_3$ and $^5D_0 \rightarrow {}^7F_4$ transitions of Eu^{3+}, respectively. The emission intensity of $^5D_0 \rightarrow {}^7F_2$ (616 nm) is much higher than that of $^5D_0 \rightarrow {}^7F_1$ (590 nm). Whereas the broad emission peaked at 434nm of Tb^{3+}@1 and 537 nm of Eu^{3+}@1 could be attributed to a π→π* transition originated from the TZI^{3-} ligand. However, other two Ln^{3+}@1 (Ln^{3+} = Dy^{3+}, Sm^{3+}) samples show a strong ligand emission band and weak characteristic emission of Dy^{3+} ions at λ_{em} = 574 nm and Sm^{3+} ions at λ_{em} = 642 nm, corresponding to the $^4F_{9/2} \rightarrow {}^6H_{13/2}$ and $^4G_{5/2} \rightarrow {}^6H_{9/2}$ transitions, respectively. Thus the energy transfer from the ligand to the lanthanide (III) ions is not so effective in Dy^{3+}@1 and Sm^{3+}@1.

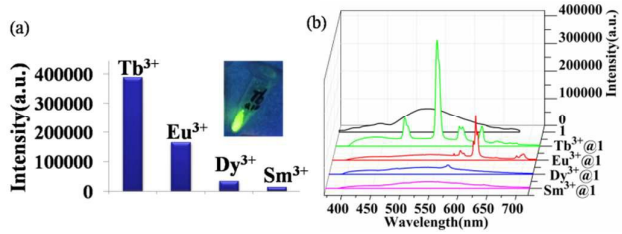

Fig.5(a) The peak intensities of the highest characteristic peak of Tb^{3+}, Eu^{3+}, Dy^{3+} and Sm^{3+} in their emission spectra. The sample of Tb^{3+}@1 illuminated with 254 nm laboratory UV light is inserted. (b) Emission spectra of compound **1**, Tb^{3+}@1, Eu^{3+}@1, Dy^{3+}@1 and Sm^{3+}@1 in the solid state at room temperature.

It should be noted that the luminescence intensity of Tb^{3+}@1 is much higher than those of Eu^{3+}@1, Dy^{3+}@1 and Sm^{3+}@1 (excitation slit: 1 nm, emission slit: 1 nm). In this context, the luminescence of the Tb^{3+}@1was measured with excitation slit: 0.5 nm and emission slit: 1 nm. Even under these conditions, the emission intensity of

the highest characteristic peak of Tb^{3+}@1 (λ_{em} = 544 nm, 387977) is much higher than those of Eu^{3+}@1 (λ_{em} = 616 nm, 164735), Dy^{3+}@1 (λ_{em} = 574 nm, 33397), and Sm^{3+}@1 (λ_{em} = 642nm, 13551) (Fig. 5a). Although the encapsulation amounts of lanthanide(III) ions are similar for Ln^{3+}@1 (Ln^{3+} = Eu^{3+}, Tb^{3+}, Dy^{3+} or Sm^{3+}), the emission intensities are greatly different. Moreover, these results indicate that **1** is suitable for the sensitization of Tb^{3+} ions rather than Eu^{3+}, Dy^{3+} and Sm^{3+} ions. Correspondingly, upon excitation with a standard UV lamp (ex = 254 nm), the Tb^{3+}@1 emitted its characteristic green color, which were readily observed with the naked eye as a qualitative indication of terbium sensitization (Fig. 5a insert).

As shown in Fig. S7, the PL decay curves of Tb^{3+}@1, Eu^{3+}@1, Dy^{3+}@1 and Sm^{3+}@1 are recorded at room temperature with emission monitored by the $^5D_4 \rightarrow {}^7F_5$ transition at 544 nm, the $^5D_0 \rightarrow {}^7F_2$ transition at 616 nm, the $^4F_{9/2} \rightarrow {}^6H_{13/2}$ transition at 574 nm and the $^4G_{5/2} \rightarrow {}^6H_{9/2}$ transition at 642 nm, respectively (λ_{ex} = 350 nm). The decay curves can be well fitted into a double exponential function: $I = I_0 + A_1 \exp(-t/\tau_1) + A_2 \exp(-t/\tau_2)$, where τ_1 and τ_2 are defined as the luminescent lifetimes. The detailed fitting results are summarized in Fig. S7.

Since compound **1** emits blue-green light, it may construct the white-light emitting materials through encapsulating Eu^{3+} ions as red emitter into **1**. The emission spectra of Eu^{3+}@l were recorded under varying UV light excitation from 310 to 394 nm (Fig. 6a). Strikingly, tunable colors and white light have been observed along with varying excitation wavelengths. When excited at 310 and 320 nm, Eu^{3+}@l mainly emits red luminescence. Upon varying the excitation light to 330 and 340 nm, the emissions display yellow light. When excited at 350 nm, the emission spectra of Eu^{3+}@l exhibit a broad emission band in the region of 400 to 570 nm of the TZI^{3-} ligand and the characteristic emission peaks centered at 579, 590, 616, 652 and 698nm of the Eu^{3+} ions (Fig. 6a). The CIE coordinates (0.320, 0.346) for Eu^{3+}@l (Fig. 6b-A) is near to the pure white value (0.333, 0.333) and the quantum yield is 3.78%. Adjusting the excitation light from 360 to 390 nm, it mainly displays green light. When excited at 394nm, near white light emission is also obtained and its CIE coordination is (0.345, 0.324) (Fig. 6b-B). The quantum yield is 2.93%. Thus, we can say that tunable colors and white-light emission were achieved by the encapsulation of Eu^{3+} ions. The emission colors at different excitation wavelengths are illustrated in the CIE chromaticity diagram (Fig. 6b), while the corresponding CIE color coordinates are listed in Table S6.

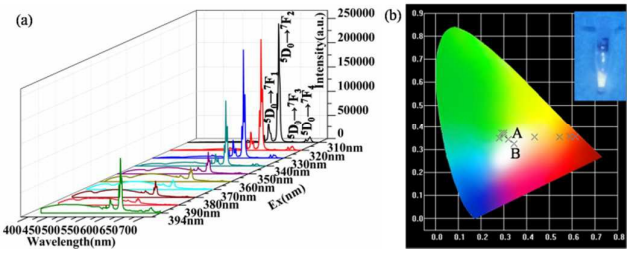

Fig.6(a) Solid-state emission spectra of Eu^{3+}@l with excitation wavelengths varying from 310 to 394 nm. (b) The CIE chromaticity diagram for Eu^{3+}@l under excitation wavelengths from 310 to 394 nm. The sample of Eu^{3+}@l illuminated with 254 nm laboratory UV light is inserted.

Eu^{3+}@1 and Tb^{3+}@1 emitted their respective red and green colors excited at 312 nm, and the samples of **1** (50 mg) immersed in water solutions of nitrate salts with different molar ratios of Eu^{3+}/Tb^{3+}: $Eu_{0.8}/Tb_{0.2}$, $Eu_{0.7}/Tb_{0.3}$, $Eu_{0.6}/Tb_{0.4}$, $Eu_{0.5}/Tb_{0.5}$, $Eu_{0.4}/Tb_{0.6}$, $Eu_{0.3}/Tb_{0.7}$, and $Eu_{0.2}/Tb_{0.8}$ (5 mL, 0.1 mol/L) displayed the tunable colors (Fig. 7b). While the corresponding CIE color coordinates are listed in Table S7. The Eu^{3+}/Tb^{3+}-loaded samples showed multiband emissions (Fig. 7a). The multiband emissions from the samples are good candidates for tunable luminescent materials.[36] As shown in Fig. 7a, the emission bands of Eu^{3+}/Tb^{3+}-loaded samples arise from $^5D_0 \rightarrow {}^7F_J$ (J = 1–4) transitions of Eu^{3+} ions ($^5D_0 \rightarrow {}^7F_1$ at 590, $^5D_0 \rightarrow {}^7F_2$ at 617, $^5D_0 \rightarrow {}^7F_3$ at 652, and $^5D_0 \rightarrow {}^7F_4$ at 699 nm) and $^5D_4 \rightarrow {}^7F_J$ (J = 6 and 5) transitions of Tb^{3+} ions ($^5D_4 \rightarrow {}^7F_6$ at 488 and $^5D_4 \rightarrow {}^7F_5$ at 544 nm).

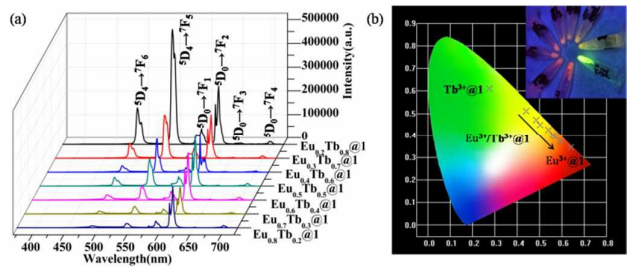

Fig.7(a) Solid-state emission spectra of Eu^{3+}/Tb^{3+}-loaded samples with excitation wavelengths at 312 nm. (b) The CIE chromaticity diagram for Tb^{3+}@1, Eu^{3+}@1 and the Eu^{3+}/Tb^{3+}-loaded samples under excitation wavelengths at 312 nm. (Insert: The sample of Tb^{3+}@1, Eu^{3+}@1 and Eu^{3+}/Tb^{3+} with different molar ratios illuminated with 254 nm laboratory UV light)

As depicted in Fig. S8a, the emission spectra of $Eu_{0.5}Tb_{0.5}$@l were recorded under varying UV light excitation from 320 to 394 nm. White light emission and color-tunable luminescence from yellow to green were realized (Fig. S8b), while the corresponding CIE color coordinates are listed in Table S8. The PL decay curves of Eu^{3+}/Tb^{3+}-loaded samples are recorded at room temperature (Fig. S9) and the detailed fitting results are summarized in Table S9.

Sensing properties

Recently, the highly efficient small-molecule sensing properties involving CPs have attracted considerable attention.[37] To explore the potential of **1** towards the sensing of small molecules, their luminescent properties were investigated in different solvent suspensions. The most interesting feature is that the PL spectra are largely dependent on the solvent molecules, particularly in the case of $CHCl_3$, which exhibits the most significant quenching effect (Fig. 8). Such solvent-dependent luminescence properties are of interest for the sensing of $CHCl_3$ solvent molecules. The different degrees of quenching effects can be ascribed to the different interaction forces

between solvents and framework of **1**, which influenced the electron transfer process.[38] In addition, the activated **1** exhibits more obviously quenching effect for bromo-substituted reagents ($CHBr_3$ and CH_2Br_2) than chloro-substituted reagents ($CHCl_3$ and CH_2Cl_2) under the same experimental conditions. Moreover, for chloro-substituted reagents, quenching effect of $CHCl_3$ is better than CH_2Cl_2 (Fig. S10). Therefore quenching might be related with electron density of the guest solvent molecule. The PXRD patterns of **1** after treating to different solvents are in agreement with the simulated one (Fig. S11).

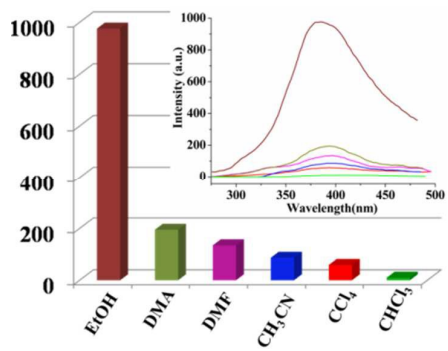

Fig.8 Comparisons of the luminescence intensity of 1-solvent emulsions at room temperature (excited at 256 nm) (insert: emission spectra of 1-solvent emulsions).

When $CHCl_3$ solvent was gradually and increasingly added to the 1-EtOH standard emulsions, the fluorescence intensities of the standard emulsions gradually decreased with the addition of the $CHCl_3$ solvent (Fig. 9). These encouraging results reveal that **1** could be promising luminescent probes for detecting small molecules of $CHCl_3$.

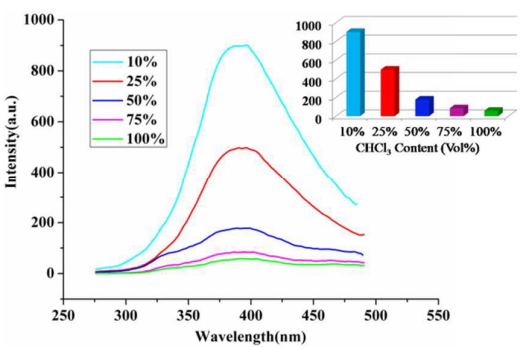

Fig.9 Emission spectra of dispersed **1** in EtOH in the presence of various amounts of $CHCl_3$ solvent (excited at 256 nm). Insert: comparisons of the luminescence intensity of different $CHCl_3$ content (Vol %).

Conclusions

In summary, using bifunctional H_3TZI ligand, three layer-structured coordination polymers (CPs) have been successfully synthesized under hydrothermal conditions, in which the ligand shows various coordination geometries. These new CPs all exhibit intensively fluorescence emissions at room temperature. Notably, **1** can function as a host for encapsulation of lanthanide (III) ions and serve as an antenna to sensitize Ln^{3+} ions, especially suitable for Eu^{3+} and Tb^{3+} ions. By encapsulating different Ln^{3+} ions, Ln^{3+}**@1** shows tunable luminescent emission including white-light emitting. In addition, **1** exhibits highly luminescent sensing properties for organic small molecules. This work indicates tetrazole–carboxylic acid ligand is in favor of the construction of functional CPs, especially in photoluminescence. Further work will be focus on the investigation of other functional CPs constructed from the H_3TZI ligand and its derivatives.

Acknowledgements

We gratefully acknowledge the financial support through the National Natural Science Foundation of China (no. 21171065 and 21201077).

Notes and references

1 (a) K. S. Jeong, Y. B. Go, S. M. Shin, S. J. Lee, J. Kim, O. M. Yaghi and N. Jeong, *Chem. Sci.*, 2011, **2**, 877; (b) T. Wu, R. Khazhakyan, L. Wang, X. H. Bu, S. T. Zheng, V. Chau and P. Y. Feng, *Angew. Chem.*, 2011, **123**, 2584; *Angew. Chem., Int. Ed.,* 2011, **50**, 2536; (c) K. Otsubo, Y. Wakabayashi, J. Ohara, S. Yamamoto, H. Matsuzaki, H. Okamoto, K. Nitta, T. Uruga and H. Kitagawa, *Nat. Mater.*, 2011, **10**, 291; (d) H. L. Jiang, B. Liu, T. Akita, M. Haruta, H. Sakurai and Q. Xu, *J. Am. Chem. Soc.*, 2009, **131**, 11302; (e) J. R. Li and H. C. Zhou, *Nat. Chem.*, 2010, **2**, 893; (f) J. R. Li, R. J. Kuppler and H. C. Zhou, *Chem. Soc. Rev.*, 2009, **38**, 1477; (g) Y. Chen, G. Li, Z. Chang, Y. Qu, Y. Zhang and X. Bu, *Chem. Sci.*, 2013, **4**, 3678.

2 (a) A. M. Shultz, O. K. Farha, J. T. Hupp and S. T. Nguyen, *J. Am. Chem. Soc.,* 2009, **131**, 4204; (b) Y. E. Cheon and M. P. Suh, *Angew. Chem.*, 2009, **121**, 2943; *Angew. Chem., Int. Ed.,* 2009, **48**, 2899; (c) B. Chen, S. Xiang and G. Qian, *Acc. Chem. Res.*, 2010, **43**, 1115; (d) R. E. Morris and X. Bu, *Nat. Chem.*, 2010, **2**, 353; (e) D. Du, J. Qin, T. Wang, S. Li, Z. Su, K. Shao, Y. Lan, X. Wang and E. Wang, *Chem. Sci.*, 2012, **3**, 705; (f) H. L. Jiang, B. Liu, Y. Q. Lan, K. Kuratani, T. Akita, H. Shioyama, F. Zong and Q. Xu, *J. Am. Chem. Soc.,* 2011, **133**, 11854.

3 (a) S. Shimomura, M. Higuchi, R. Matsuda, K. Yoneda, Y. Hijikata, Y. Kubota, Y. Mita, J. Kim, M. Takata and S. Kitagawa, *Nat. Chem.,* 2010, **2**, 633; (b) Y. F. Zeng, X. Hu, F. C. Liu and X. H. Bu, *Chem. Soc. Rev.*, 2009, **38**, 469; (c) J. J. Jang, L. Li, T. Yang, D. B. Kuang, W. Wang and C. Y. Su, *Chem. Commun.,* 2009, **17**, 2387; (d) A. J. Cairns, J. A. Perman, L. Wojtas, V. Ch. Kravtsov, M. H. Alkordi, M. Eddaoudi and M. J. Zaworotko, *J. Am. Chem. Soc.*, 2008, **130**, 1560; (e) F. J. M. Hoeben, P. Jonkheijm, E. W. Meijer, A. P. H. J. Schenning, *Chem. Rev.*, 2005, **105**, 1491; (f) X. H. Bu, M. L. Tong, H. C. Chang, S. Kitagawa and S. R. Batten, *Angew. Chem., Int. Ed.*, 2004, **43**, 192.

4 (a) L. E. Kreno, K. Leong, O. K. Farda, M. Allendorf, R. P. Van Duyne and J. T. Hupp, *Chem. Rev.*, 2012, **112**, 1105; (b) H. L. Jiang, Y. Tatsu, Z. H. Lu and Q. Xu, *J. Am. Chem. Soc.*, 2010, **132**, 5586; (c) J. D. Xiao, L. G. Qiu, F. Ke, X. P. Yuan, G. S. Xu, Y. M. Wang and X. Jiang, *J. Mater. Chem. A.*, 2013, **1**, 8745; (d) B. L. Chen, L. B. Wang, Y. Q. Xiao, F. R. Fronczek, M. Xue, Y. J. Cui and G. D. Qian, *Angew. Chem., Int. Ed.*, 2009, **28**, 500; (e) Z. Hu, B. J. Deibert and J. Li, *Chem. Soc. Rev.*, 2014,

43, 5815; (f) Y. N. Gong, L. Jiang and T. B. Lu, *Chem. Commun.*, 2013, **49**, 11113; (g) Z. Guo, H. Xu, S. Su, J. Cai, S. Dang, S. Xiang, G. Qian, H. Zhang, M. O'Keeffe and B. Chen, *Chem. Commun.*, 2011, **47**, 5551; (h) P. Zhou, D. Zhou, L. Tao, Y. Zhu, W. Xu, S. Xu, S. Cui, L. Xu and H. Song, *Light Sci. Appl.*, 2014, **3**, e209.

5 (a) Y. Q. Lan, H. L. Jiang, S. L. Li and Q. Xu, *Inorg. Chem*., 2012, **51**, 7484; (b) R. M. Abdelhameed, L. D. Carlos, A. M. S. Silva and J. Rocha, *Chem. Commun*., 2013, **49**, 5019; (c) Y. Lu and B. Yan, *Chem. Commun*., 2014, **50**, 9969; (d) Y. Zhou and B. Yan, *J. Mater. Chem. A*., 2014, 2, 13691.

6 (a) R. C. Huxford, J. Della Rocca and W. B. Lin, *Curr. Opin. Chem. Biol*., 2010, **14**, 262; (b) D. Cunba, M. Ben Yahia, S. Hall, S. R. Miller, H. Chevreau, E. Elkaim, G. Maurin, P. Horcajada and C. Serre, *Chem. Mater*., 2013, **25**, 2767; (c) K. M. L. Taylor, W. J. Rieter and W. B. Lin, *J. Am. Chem. Soc*., 2008, **130**, 14358; (d) Y. Lu and B. Yan, *J. Mater. Chem. C*., 2014, **2**, 7411.

7 P. Falcaro and S. Furukawa, *Angew. Chem., Int. Ed.,* 2012, **51**, 8431.

8 Y. Cui, H. Xu, Y. Yue, Z. Guo, J. Yu, Z. Chen, J. Gao, Y. Yang, G. Qian and B. Chen, *J. Am. Chem. Soc*., 2012, **134**, 3979.

9 D. F. Sava, L. E. Rohwer, M. A. Rodriguez and T. M. Nenoff, *J. Am. Chem. Soc.*, 2012, **134**, 3983.

10 W. Xie, S. R. Zhang, D. Y. Du, J. S. Qin, S. J. Bao, J. Li, Z. M. Su, W. W. He, Q. Fu and Y. Q. Lan, *Inorg. Chem*., 2015, **54**, 3290.

11 F. Luo and S. R. Batten, *Dalton Trans*., 2010, **39**, 4485.

12 Y. Q. Lan, H. L. Jiang, S. L. Li and Q. Xu, *Adv. Mater.*, 2011, **23**, 5015.

13 Y. Wang, J. Yang, Y. Y. Liu and J. F. Ma, *Chem. –Eur. J.*, 2013, **19**, 14591.

14 J. An, C. M. Shade, D. A. Chengelis-Czegan, S. Petoud and N. L. Rosi, *J. Am. Chem. Soc.*, 2011, **133**, 1220.

15 L. Chen, K. Tan, Y. Q. Lan, S. L. Li, K. Z. Shao and Z. M. Su, *Chem. Commun.*, 2012, **48**, 5919.

16 F. Luo, M. S. Wang, M. B. Luo, G. M. Sun, Y. M. Song, P. X. Li and G. C. Guo, *Chem. Commun*., 2012, **48**, 5989.

17 Q. B. Bo, H. Y. Wang, D. Q. Wang, Z. W. Zhang, J. L. Miao and G. X. Sun, *Inorg. Chem.*, 2011, **50**, 10163.

18 C. X. Chen, Q. K. Liu, J. P. Ma and Y. B. Dong, *J. Mater. Chem.*, 2012, **22**, 9027.

19 H. Zhang, P. Lin, X. Shan, F. Du, Q. Li and S. Du, *Chem. Commun.*, 2013, **49**, 2231.

20 Y. Y. Jiang, S. K. Ren, J. P. Ma, Q. K. Liu and Y. B. Dong, *Chem. Eur. J*., 2009, **15**, 10742.

21 J. S. Qin, S. R. Zhang, D. Y. Du, P. Shen, S. J. Bao, Y. Q. Lan and Z. M. Su, *Chem. Eur. J*., 2014, **20**, 5625.

22 a) K. A. Hirsch, S. R. Wilson and J. S. Moore, *Inorg. Chem*., 1997, **36**, 2960; b) M. Munakata, L. P. Wu, T. Kuroda-Sowa, M. Maekawa, K. Moriwaki and S. Kitagawa, *Inorg. Chem.*, 1997, **36**, 5416; c) X. H. Bu, W. Chen, W. F. Hou, M. Du, R. H. Zhang and F. Brisse, *Inorg. Chem*., 2002, **41**, 3477; d) M. Dinca, A. F. Yu and J. R. Long, *J. Am. Chem. Soc.*, 2006, **128**, 8904.

23 Y. Wang, J. Yang, Y. Y. Liu and J. F. Ma, *Chem. Eur. J.*, 2013, **19**, 14591.

24 A. J. Calahorro, A. S. Castillo, J. M. Seco, J. Zuñiga, E. Colacio and A. R. Diéguez, *CrystEngComm.*, 2013, **15**, 7636.

25 (a) F. Nouar, J. F. Eubank, T. Bousquet, L. Wojtas, M. J. Zaworotko and M. Eddaoudi, *J. Am. Chem*., Soc. 2008, **130**, 1833; (b) H. K. Chae, J. Kim, O. D. Friedrichs, M. O'Keeffe and O. M. Yaghi, *Angew. Chem., Int. Ed*., 2003, **42**, 3907; (c) H. Furukawa, M. A. Millerb and O. M. Yaghi, *J. Mater. Chem.*, 2007, **17**, 3197; (d) S. Wang, J. L. Zuo, S. Gao, Y. Song, H. C. Zhou, Y. Z. Zhang and X. Z. You, *J. Am. Chem., Soc.*, 2004, **126**, 8900.

26 (a) H. Zhao, Z. R. Qu, H. Y. Ye and R. G. Xiong, *Chem. Soc. Rev.*, 2008, **37**, 84; (b) A. F. Stassen, M. Grunert, A. M. Mills, A. L. Spek, J. G. Haasnoot, J. Reedijk and W. Linert, *Dalton Trans.*, 2003, **18**, 3628; (c) J. Tao, Z. J. Ma, R. B. Huang, L. S. Zheng, *Inorg. Chem*., 2004, **43**, 6133; (d) C. Jiang, Z. Yu, C. Jiao, S. Wang, J. Li, Z. Wang and Y. Cui, *Eur. J. Inorg. Chem*., 2004, **23**, 4669; (e) T. T. Luo, H. L. Tsai, S. L. Yang, Y. H. Liu, R. DayalYadav, C. C. Su, C. H. Ueng, L. G. Lin and K. L. Lu, *Angew. Chem., Int. Ed.,* 2005, **44**, 6063; (f) M. Dinca, A. F. Yu and J. R. Long, *J. Am. Chem. Soc*., 2006, **128**, 8904; (g) J. R. Li, Y. Tao, Q. Yu and X. H. Bu, *Chem. Commun*., 2007, **15**, 1527; (h) J. R. Li, Q. Yu, E. C. Sañudo, Y. Tao, W. C. Song and X. H. Bu, *Chem. Mater*., 2008, **20**, 1218; (i) R. Antonio, K. Raikko and C. Enrique, *Chem. Commun.*, 2005, **41**, 5228.

27 T. Smith and J. Guild, *Trans. Opt. Soc.*, London 1931, **33**, 73.

28 G. M. Sheldrick, SHELXS-97: Programs for Crystal Structure Solution, University of Götingen: Götingen (Germany), 1997.

29 (a) V. A. Blatov, L. Carlucci, G. Ciani and D. M. Proserpio, *CrystEngComm*, 2004, **6**, 378; (b) V. A. Blatov, A. P. Shevchenko and V. N. Serezhkin, *Acta Crystallogr., Sect. A: Found. Crystallogr.*, 1995, **51**, 909.

30 D. X. Xue, Y. Y. Lin, X. N. Cheng and X. M. Chen, *Crystal Growth & Design,* 2007, **7**, 1332.

31 Y. Bai, G. J. He, Y. G. Zhao, C. Y. Duan, D. B. Dang and Q. J. Meng, *Chem. Commun.*, 2006, **14**, 1530.

32 J. Jia, J. N. Xu, S. Y. Wang, P. C. Wang, L. J. Gao, M. Yu, Y. Fan and L. Wang, *CrystEngComm*, 2015, 17, 6030–6036.

33 (a) P. C. Ford and A. Vogler, *Acc. Chem. Res*., 1993, **26**, 220; (b) A. Vogler, A. Paukner and H. Kunkely, *Coord. Chem. Rev.*, 1980, **33**, 227; (c) H. Nikol, A. Becht and A. Vogler, *Inorg. Chem.*, 1992, **31**, 3277.

34 Y. Cui, Y. Yue, G. Qian and B. Chen, *Chem. Rev.*, 2012, **112**, 1126.

35 G. Blasse and B. C. Grabmaier, Luminescent Materials, Springer, Berlin, 1994.

36 K. A. White, D. A. Chengelis, K. A. Gogick, J. Stehman, N. L. Rosi and S. Petoud, *J. Am. Chem. Soc.*, 2009, **131**, 18069.

37 S. S. Nagarkar, B. Joarder, A. K. Chaudhari, S. Mukherjee and S. K. Ghosh, *Angew. Chem., Int. Ed.*, 2013, **52**, 2881.

38 (a) H. Wang, W. T. Yang and Z. M. Sun, *Chem. Asian J.*, 2013, **8**, 982. (b) D. Tian, Y. Li, R. Y. Chen, Z. Chang, G. Y. Wang and X. H. Bu, *J. Mater. Chem. A*, 2014, **2**, 1465.

Graphical Abstract

Compound **1** can play as a host for encapsulation of Ln^{3+} ions.